Induction of transient macroapertures in endothelial cells through RhoA inhibition by *Staphylococcus aureus* factors

Laurent Boyer,[1] Anne Doye,[1] Monica Rolando,[1] Gilles Flatau,[1] Patrick Munro,[1] Pierre Gounon,[3] René Clément,[1] Céline Pulcini,[1] Michel R. Popoff,[6] Amel Mettouchi,[2] Luce Landraud,[1,4] Olivier Dussurget,[5] and Emmanuel Lemichez[1]

[1]Toxines Bactériennes dans la Relation Hôte-Pathogènes, U627, and [2]Biologie et Physiopathologie Cutanée, Faculté de Médecine, Institut National de la Santé et de la Recherche Médicale, INSERM, 06107 Nice Cedex 2, France
[3]Centre Commun de Microscopie Électronique Appliquée, Faculté des Sciences, 06108 Nice Cedex 2, France
[4]Laboratoire Central de Bactériologie, Hôpital ARCHET II, 06202 Nice Cedex 3, France
[5]Unité des Interactions Bactéries-Cellules, Institut National de la Santé et de la Recherche Médicale, INSERM, U604, and [6]Unité des Bactéries Anaérobies et Toxines, Institut Pasteur, 75015 Paris, France

The GTPase RhoA is a major regulator of the assembly of actin stress fibers and the contractility of the actomyosin cytoskeleton. The epidermal cell differentiation inhibitor (EDIN) and EDIN-like ADP-ribosyltransferases of *Staphylococcus aureus* catalyze the inactivation of RhoA, producing actin cable disruption. We report that purified recombinant EDIN and EDIN-producing *S. aureus* provoke large transcellular tunnels in endothelial cells that we have named macroapertures (MAs). These structures open transiently, followed by the appearance of actin-containing membrane waves extending over the aperture. Disruption of actin cables, either directly or indirectly, through *rhoA* RNAi knockdown also triggers the formation of MAs. Intoxication of endothelial monolayers by EDIN produces a loss of barrier function and provides direct access of the endothelium basement membrane to *S. aureus*.

Introduction

The Rho, Rac, and Cdc42 GTPases of the Rho protein family integrate environmental signals to regulate the organization and dynamic of the actin cytoskeleton (Burridge and Wennerberg, 2004; Jaffe and Hall, 2005). This confers to Rho proteins a direct role in controlling cell shape and adhesion, which are two key determinants in the regulation of the barrier function of the endothelium and epithelium (Wojciak-Stothard and Ridley, 2002). Hence, the major role played by Rho proteins accounts for the existence of a large number of bacterial virulence factors targeting them (Boquet and Lemichez, 2003).

Rho proteins oscillate between a GDP-bound form sequestered in the cytosol, in association with the cellular factor Rho guanine nucleotide dissociation inhibitor (RhoGDI; DerMardirossian and Bokoch, 2005), and a GTP-bound form that is found in specific membrane locations, which bind and activate effector proteins (Burridge and Wennerberg, 2004). Transitions between both forms of Rho are primarily regulated by guanine nucleotide exchange factors for activation and GTPase-activating proteins for inactivation (Burridge and Wennerberg, 2004). Rho protein isoforms specifically regulate the architecture and dynamic of the actin cytoskeleton (Burridge and Wennerberg, 2004; Jaffe and Hall, 2005). The activation of Rac or Cdc42 leads to actin filament polymerization, forming actin-rich lamellipodia or filopodia, respectively. RhoA induces actomyosin contraction and the formation of actin stress fibers by controlling the phosphorylation status of the myosin light chain (MLC). Phosphorylation of MLC is controlled by MLC kinases and Rho kinases (ROCKs; Katoh et al., 2001; Burridge and Wennerberg, 2004). Activation of ROCKs by RhoA primarily leads the phosphorylation/inactivation of the regulatory subunit of the myosin-specific phosphatase MYPT1 (Kimura et al., 1996). Thus, Rho regulates different aspects of the organization of the actin cytoskeleton in differentiated cells that impact their morphology, as well as both intercellular and cell–matrix adhesion (Burridge and Wennerberg, 2004; Jaffe and Hall, 2005). For instance, the activation of Rho by vasoactive factors such as thrombin induces actomyosin contractions that are responsible, in part, for destabilizing the endothelial intercellular junctions

L. Boyer and A. Doye contributed equally to this paper

Correspondence to Emmanuel Lemichez: lemichez@unice.fr

Abbreviations used in this paper: EDIN, epidermal cell differentiation inhibitor; HMVEC, human microvascular endothelial cell; HUVEC, human umbilical vein endothelial cell; MA, macroaperture; RhoGDI, Rho guanine nucleotide dissociation inhibitor; ROCK, Rho kinase; SFM, serum-free medium; VVO, vesiculo-vacuolar organelle; WGA, wheat germ agglutinin.

The online version of this article contains supplemental material.

The Journal of Cell Biology, Vol. 173, No. 5, June 5, 2006 809–819
http://www.jcb.org/cgi/doi/10.1083/jcb.200509009

and promoting the formation of intercellular gaps through cell contraction (Wojciak-Stothard and Ridley, 2002). Hence, recent findings indicate that Rho proteins of endothelial cells participate in leukocyte transmigration across the endothelium (Carman and Springer, 2004; Millan and Ridley, 2005). In columnar epithelial cells, Rho promotes the formation of actin filaments associated with apical tight junctions and in so doing contributes to epithelium cohesion (Nusrat et al., 1995).

Staphylococcus aureus epidermal cell differentiation inhibitor (EDIN; Sugai et al., 1990) and EDIN-like factors (Aktories et al., 2004) belong to a family of ADP-ribosyltransferases that are expressed both by human and animal Gram-positive pathogenic bacteria (Aktories et al., 2004). They consist of a single polypeptide chain, which penetrates host cells by an undefined molecular mechanism. Upon reaching the host cell cytosol, these factors catalyze the preferential ADP-ribosylation of RhoA (Chardin et al., 1989; Aktories et al., 2004) and, to a lesser extent, other isoforms of Rho proteins (Wilde et al., 2003). Posttranslational modification of Rho by ADP-ribosylation leads to the tight association of RhoA with RhoGDI, leading to Rho sequestration into the cytosol (Fujihara et al., 1997; Genth et al., 2003). In addition, ADP-ribosylation blocks RhoA activation by the guanine nucleotide exchange factor lbc (Aktories et al., 2004). The inhibitory effects of RhoA ADP-ribosylation by EDIN-like factors lead to the disruption of actin stress fibers (Chardin et al., 1989; Paterson et al., 1990; Aktories et al., 2004).

Major progress has been made in understanding how bacterial Rho ADP-ribosylating factors interfere with immune cells (Caron and Hall, 1998; Aktories et al., 2004). To gain more insights on the biological activity of EDIN-like factors, we have investigated the effects of purified recombinant EDIN, as well as EDIN-producing *S. aureus*, on endothelial cells and on the endothelium.

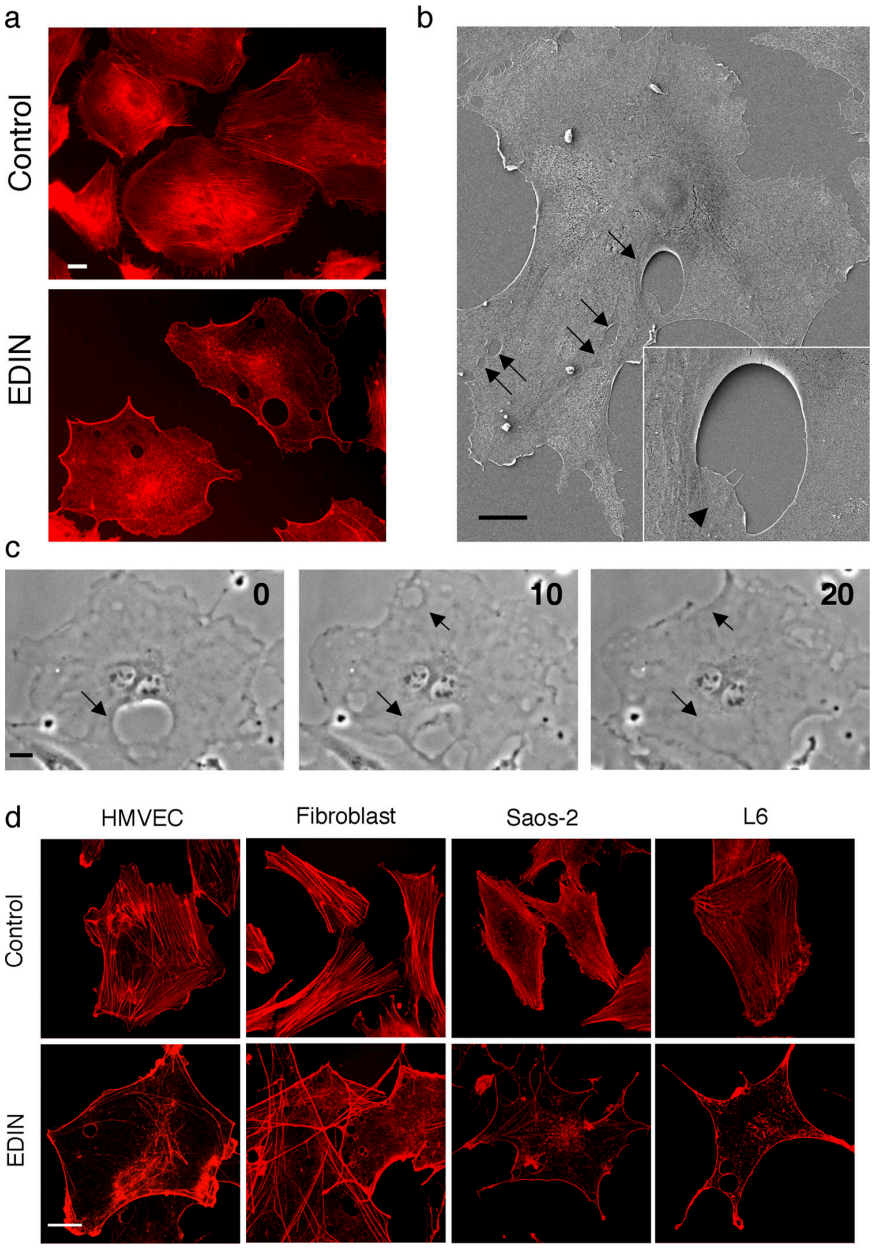

Figure 1. **EDIN induces the formation of transient MAs.** (a) Actin cytoskeleton disruption and MA formation in HUVECs intoxicated for 24 h with 100 μg/ml of EDIN. The actin cytoskeleton was visualized using TRITC-conjugated phalloidin. (b) Visualization of MAs (arrows) by scanning electron microscopy. Inset shows a lamellipodia-like structure extending from the edge of a MA (arrowhead). HUVECs were intoxicated for 24 h with 100 μg/ml of EDIN. (c) Time-lapse video microscopy of HUVECs intoxicated with 100 μg/ml of EDIN showing MA opening and closure (arrows; images selected from Video 1; intervals in minutes). (d) Induction of MAs in different cell types intoxicated for 24 h with 100 μg/ml of EDIN. The primary human cells used were HMVECs and fibroblasts. The cell lines used were osteosarcoma-derived epithelial Saos-2 cells and myoblast L6 cells. The actin cytoskeleton was visualized using FITC- or TRITC-conjugated phalloidin. Color balance was adjusted in red. Video 1 is available at http://www.jcb.org/cgi/content/full/jcb.200509009/DC1. Bars, 10 μm.

Results

Rho ADP-ribosylation induces transient macroapertures (MAs)

We have observed that intoxication of human umbilical vein endothelial cells (HUVECs) with purified recombinant EDIN results in the formation of large transcellular tunnels that we have named MAs, in addition to the previously described dislocation of actin stress fibers (Fig. 1, a and b; Chardin et al., 1989; Paterson et al., 1990). We noticed the presence of membranes extending from the edge of MAs (Fig. 1 b, inset, arrowhead). Analysis of the intoxication of HUVECs by EDIN, using time-lapse video microscopy, revealed the transient nature of MAs (Fig. 1 c; and Video 1, available at http://www.jcb.org/cgi/content/full/jcb.200509009/DC1). Complete cycles of MA opening and closure took 2–20 min, with a mean time of 12 min ($n = 45$ MAs, at 24 h of intoxication). In contrast, no MAs were observed in control HUVECs. EDIN also produced MAs in other potential targets of *S. aureus*, such as primary human microvascular endothelial cells and fibroblasts, as well as the myoblast and osteoblast cell lines L6 and Saos-2, respectively (Fig. 1 d). A low occurrence of MAs was observed in EDIN-treated human keratinocytes and columnar epithelial T84 subconfluent cells (MAs $\leq 2\%$ at 48 h; unpublished data).

We next investigated the characteristics of MA induction by EDIN in subconfluent endothelial cells. MAs were detected 3 h after cell intoxication and progressively affected 33% of the cell population after 24 h of intoxication (Fig. 2 a). The efficiency of MA formation was compared with that of Rho ADP-ribosylation, as well as inhibition of Rho activity. Correlative analysis of these kinetics indicated that MAs induced by EDIN began 3 h postintoxication concomitantly with ADP-ribosylation of 75% of endogenous Rho and 58.2% inhibition of Rho activity (Fig. 2 a). In further studying this newly described effect of EDIN, we determined that the number of cells displaying MAs increases as a function of the concentration of EDIN (Fig. 2 b). Previous studies had shown that cells recover their actin stress fibers upon Rho resynthesis, which occurs after Rho ADP-ribosylating toxin clearing (Aktories et al., 2004). Consistently, we also observed that endothelial cells recovered their initial status within 48 h after EDIN clearing (Fig. 2 c). Induction of MAs by EDIN is, thus, a time- and dose-dependent phenomenon. In addition, no effect was observed with the catalytically inactive $EDIN_{R185E}$ mutant (Fig. 2 d; Menetrey et al., 2002). Further analyzing these aspects on endothelial cells transfected with either EDIN or $EDIN_{R185E}$ expression plasmids, we observed a disruption of actin cables and the formation of MAs, specifically in cells expressing functional EDIN (Fig. 2 e). This allowed us to establish, after cell fixation and actin cytoskeleton staining, that 24 h of expression of EDIN leads to a loss of actin cables in 91% of the cells and formation of MAs in 49% of these cells ($n = 200$). Thus, consistent with the transient formation of MAs, which was observed using video microscopy, after cell fixation we found

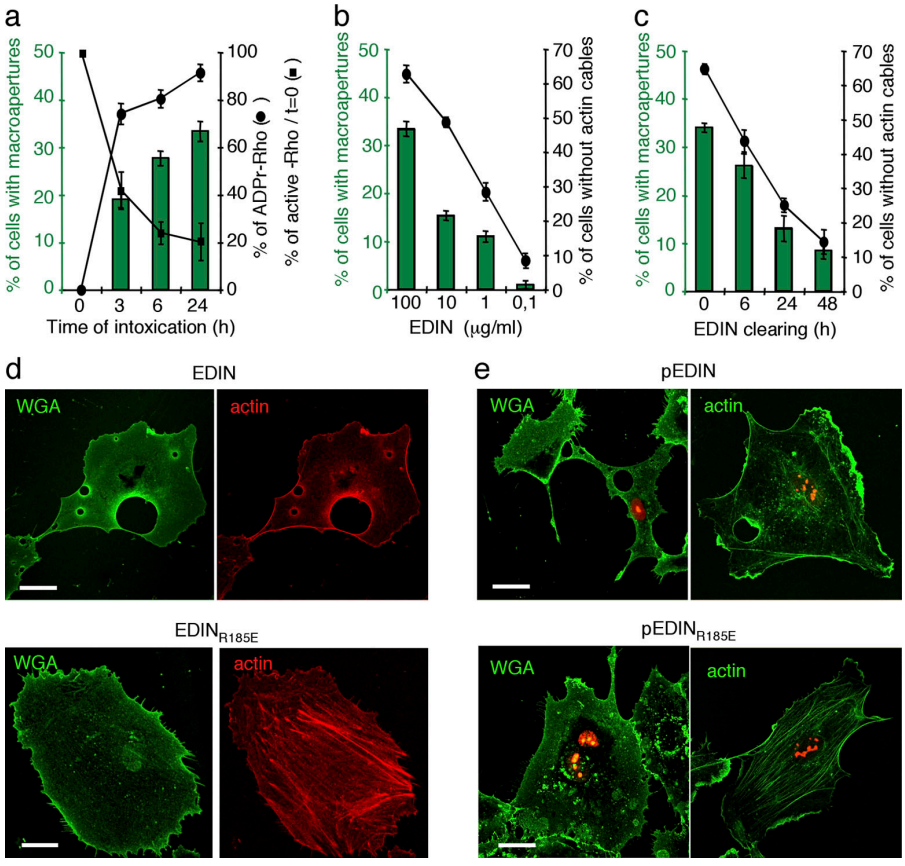

Figure 2. **Characteristics of EDIN-induced actin-cable disruption and MA formation in endothelial cells.** (a) Efficiency of MA induction in HUVECs, as compared with ADP-ribosylation and inactivation of Rho. Histogram represents the percentage of HUVECs displaying at least one MA. Mean values ± SD. $n = 3$. Cells were cultured in subconfluent conditions and intoxicated with 100 µg/ml of EDIN during the indicated periods of time. Levels of cellular ADP-ribosylated Rho (ADPr-Rho) were determined by in vitro ADP-ribosylation. Percentages represent the quenching of in vitro ADP-ribosylated Rho assessed at the indicated periods of cell intoxication by EDIN. Mean values ± SD. $n = 3$. Immunosignals of active Rho were normalized on total Rho and expressed as a percentage of active Rho compared with the control t = 0. Mean values ± SD. $n = 3$. (b and c) Percentages of HUVECs displaying at least one MA or devoid of actin cables. Percentages were determined on TRITC-phalloidin–labeled cells in three independent experiments and expressed as mean values ± SD. Subconfluent cells were intoxicated either with the indicated doses of EDIN for 24 h (b) or were intoxicated for 24 h before EDIN clearing (t = 0; c). (d and e) Plasma membrane of HUVECs was visualized using FITC-conjugated WGA. Actin cytoskeleton (actin) was visualized using either TRITC- (d) or FITC-conjugated (e) phalloidin. (d) HUVECs intoxicated for 24 h with 100 µg/ml of either EDIN or $EDIN_{R185E}$. (e) HUVECs transfected with either pEDIN or $pEDIN_{R185E}$ for 16 h. Coexpression of nucleus-targeted DsRed was used to label transfected cells. Bars, 10 µm.

that a maximal effect of EDIN produces MAs that are visible in nearly half of HUVECs.

Using video microscopy, we next analyzed the formation of MAs in cells transfected with EDIN together with GFP-caveolin1. Plasma membrane was labeled with TRITC-conjugated wheat germ agglutinin (WGA). MAs induced by EDIN appeared to result from the enlargement of a pore associated with the formation of retraction filaments (Fig. 3 a; and Video 2, available at http://www.jcb.org/cgi/content/full/jcb.200509009/DC1). Membrane retraction produces a local and transient accumulation of GFP-caveolin1 at the edge of the aperture. Rho ADP-ribosylation factors have been extensively studied using cell lines displaying thick actin cables, such as VERO cells. We noticed the formation of curved membrane "retractions" in VERO cells expressing EDIN (Fig. 3 b, arrows), which appeared to occur at the cell periphery (Video 3). Thus, at the difference with HUVECs in which EDIN induced MAs in VERO cells, membrane retractions occur at the edges of cells, leading to cellular retractions. We next investigated whether MAs were initiated by membrane ruptures. Induction of membrane wounding by pathogens or mechanical stress leads to lysosomal exocytosis for membrane repair (Roy et al., 2004). In contrast with what was reported for wounded cells (Huynh et al., 2004), the lysosomal marker Lamp1 was not detected at the cell surface of EDIN-intoxicated cells (Fig. 3c). Finally, we observed that membrane waves, which formed at the edge of apertures, contained Rac, cortactin, and Arp3 machinery of actin polymerization (Fig. 3 d), as observed in membrane ruffles (Weed et al., 1998).

MAs result from RhoA inhibition and actin stress fiber disruption

EDIN and other isoforms of the C3 exoenzyme family ADP-ribosylate RhoA and, to a lesser extent, different combinations of other Rho proteins (Wilde et al., 2003). For this reason, we examined the effects of expression of three other members of the C3 exoenzyme family, i.e., EDIN-B and -C of *S. aureus*, as well as the C3 exoenzyme of *Clostridium botulinum*. Expression of these isoforms of C3 exoenzyme also induced the formation of MAs (Fig. 4 a), in contrast with catalytically inactive mutants (Fig. S1, available at http://www.jcb.org/cgi/content/full/jcb.200509009/DC1). MAs produced by C3 exoenzyme of *C. botulinum* also formed transiently (Video 4). Collectively, these results suggested that RhoA inhibition may account for

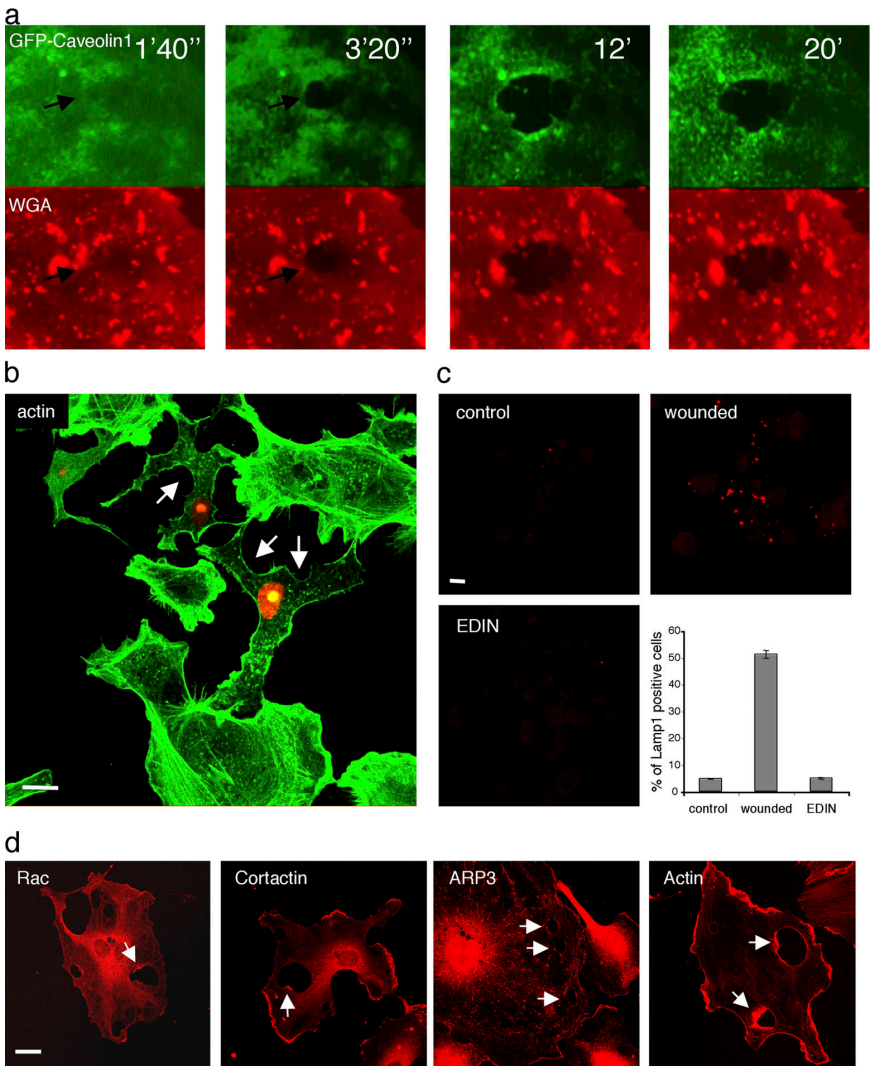

Figure 3. **Visualization of MA formation.** (a) Formation of MAs (arrows) in HUVECs cotransfected with GFP-caveolin1 and EDIN expression plasmids. Plasma membrane was labeled for 1 h with 20 μg/ml TRITC-conjugated WGA (images selected from Video 2; intervals in minutes). Contrast and color balance were adjusted. (b) Actin cytoskeleton disruption and cell retraction (arrows) in VERO cells cotransfected with pEDIN and pDsRed2 nucleus (red). Actin cytoskeleton was visualized using FITC-conjugated phalloidin (green). (c) Lysosomal exocytosis were visualized by anti-Lamp1 immunolabeling on HUVECs control, intoxicated for 24 h with 100 μg/ml of EDIN (EDIN), or wounded by electroporation at 300 V, 450 μF (wounded), as previously described (Huynh et al., 2004). Graph represents the percentage of Lamp1-positive cells. $n > 400$ cells/condition. (d) Localization of Rac, cortactin, Arp3, and actin in membrane ruffles extending from the edges of MAs (arrows). HUVECs were cotransfected with pEDIN and pEGFP (not depicted). Cells were processed for immunolabeling 16 h after transfection. Video 2 is available at http://www.jcb.org/cgi/content/full/jcb.200509009/DC1. Bars, 10 μm.

a general mechanism by which MAs are produced. To address this question we knocked down RhoA using RNA interference. The cellular depletion of RhoA was quantified by immunoblotting, and its level was found to decrease to 25% within 24 h after cell transfection (Fig. 4 b). Under these conditions, we observed that 24 h after transfection of a *rhoA* RNAi expression plasmid, endothelial cells displayed MAs and a disruption of actin cables (Fig. 4 c). The effects of RNAi-mediated RhoA knockdown on the dynamic of the actin cytoskeleton was further analyzed in endothelial cells expressing a GFP-actin chimeric molecule. In control cells, the GFP-actin signal shows actin cables and cortical actin cytoskeleton (Fig. S2 a). In endothelial cells cotransfected with *rhoA* RNAi and GFP-actin expression plasmids, MA formation appeared to be rapidly followed by the recruitment of GFP-actin around the aperture (Fig. 4 d; Video 5). GFP-actin next concentrated into lamellipodia-like structures extending from the edge of the aperture. The absence of effects of control RNAi on the actin cytoskeleton was verified (Fig. S2 b). The dynamics of the actin cytoskeleton during a cycle of MA formation by EDIN appeared similar to those observed after RNAi-mediated RhoA knockdown (Video 6). Collectively, this demonstrated that RNAi-mediated RhoA knockdown recapitulated the effects of EDIN, resulting in transient formation of MAs in endothelial cells. Our results favor the hypothesis that the destruction of cytosolic actin cables after RhoA inhibition leads to the formation of MAs. To test this hypothesis, HUVECs were treated with different drugs that destabilize the actin cytoskeleton, using mild conditions to minimize cell retractions. Under these conditions, MAs were observed upon cell treatment with cytochalasin D and latrunculin B, as well as with the ROCK inhibitor Y-27632 (Fig. 4 e). Finally, we verified that Y-27632 did not produce RhoA inhibition (not depicted),

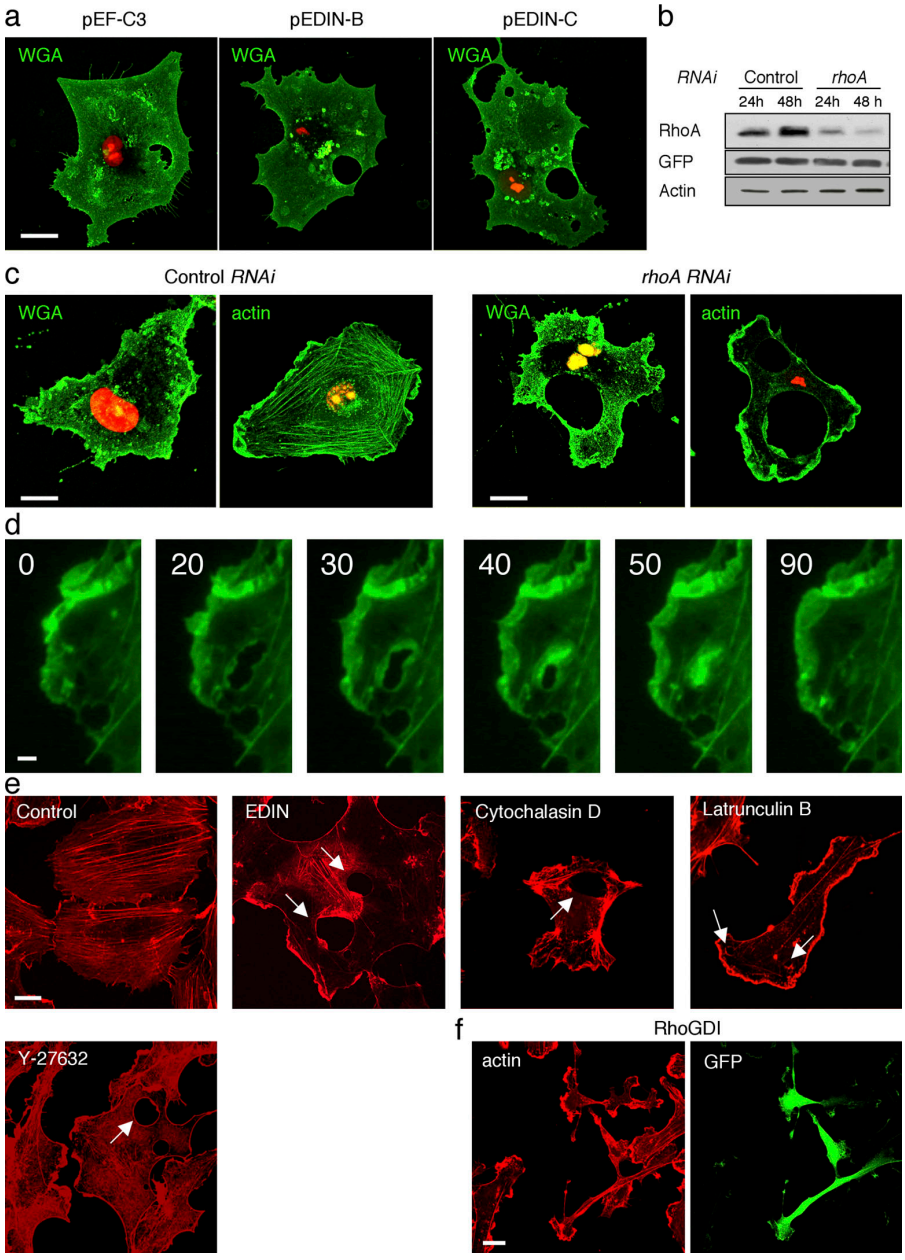

Figure 4. **Inhibition of RhoA or actin stress fiber disruption induce MAs in endothelial cells.** (a–c) HUVEC plasma membrane or actin cytoskeleton were visualized using FITC-conjugated WGA or FITC-conjugated phalloidin (actin), respectively. Coexpression of nucleus-targeted DsRed was used to label transfected cells. (a) HUVECs transfected with either pEF-C3, pEDIN-B, or -C. (b) Immunoblots showing the depletion of RhoA induced by RNAi-mediated RhoA knockdown. Cells were cotransfected with plasmids expressing either *rhoA* RNAi or *rhoA-scrambled* RNAi (control) together with pEGFP for transfection level normalization. (c) Cellular effects of RNAi-mediated RhoA knockdown 16 h after HUVECs transfection. Cells were transfected with either *rhoA* RNAi or control RNAi expression plasmids. (d) HUVECs cotransfected with GFP-actin and *rhoA* RNAi expression plasmids (images from video 6; intervals in seconds). (e) Formation of MAs (arrows) in subconfluent HUVECs treated for 7 h with 50 μM Y-27632 or 40 ng/ml latrunculin B and for 24 h with either 20 ng/ml cytochalasin D or 100 μg/ml EDIN. Efficiencies of MA formation were assessed on phalloidin-labeled cells, giving 1% for latrunculin B and cytochalasin D and 11.3% for Y-27632. n = 300 cells; two independent experiments. Actin cytoskeleton was visualized using FITC- or TRITC-conjugated phalloidin. Color balance was adjusted in red. (f) Effects of RhoGDI expression on actin cytoskeleton and cell morphology. HUVECs were cotransfected with 5 μg pRhoGDI and 10 μg pEGFP-C1. Actin cytoskeleton was visualized using TRITC-conjugated phalloidin, 6 h after cell transfection. Video 6 is available at http://www.jcb.org/cgi/content/full/jcb.200509009/DC1. Bars, 10 μm.

but, instead, dynamic MAs similar to those produced by EDIN (Fig. S2 c). In addition, we observed that the overexpression of the Rho-family inhibitor RhoGDI produced cellular retractions instead of MAs (Fig. 4 f), as does the RhoA, Rac, and Cdc42 inhibitory toxin-B of *Clostridium difficile* (Video 7; Just et al., 1995). In conclusion, we show that the preferential inhibition of RhoA by EDIN and the disruption of RhoA-regulated actin cytoskeleton account for MA formation.

Formation of MAs in endothelial cell monolayers and endothelium

We next investigated MA induction by EDIN in endothelial cell monolayers. Intercellular junctions were visualized by staining VE-cadherin, which is a major component of endothelial adherens junctions (Fig. 5 a; Bazzoni and Dejana, 2004). When HUVECs were engaged in intercellular junctions, we measured a 20% higher level of active Rho, as compared with that measured in subconfluent cells ($n = 3$, mean value). Under these conditions, we measured that the level of active Rho dropped to 0.2% of total Rho at 48 h, a value similar to that obtained with subconfluent cells intoxicated for 24 h (Fig. 5 b). In HUVEC monolayers, at 48 h of intoxication by EDIN we measured that 5.9 ± 0.5% ($n = 400$ cells) of cells displayed MAs (Fig. 5 c). MAs were also observed in human microvascular endothelial cell (HMVEC) monolayers that were intoxicated for 48 h in similar conditions (Fig. 5 d; 6.9 ± 1%; $n = 300$ cells). In contrast, no MAs were observed in HUVEC and HMVEC monolayers treated with $EDIN_{R185E}$ (unpublished data). Similar results were obtained with the C3 exoenzyme of *C. botulinum* (unpublished data). The VE-cadherin signal was not detected at the edge of MAs (Fig. 5, a and d; and Video 8, available at http://www.jcb.org/cgi/content/full/jcb.200509009/DC1). MAs also formed transiently in monolayers (Videos 8 and 9). We next investigated the effects of EDIN on endothelial monolayer barrier function. Previous studies had established that RhoA activation by vasoactive factors, such as thrombin, leads to stress fiber formation and actomyosin contractions, which are responsible for intercellular gaps opening (Essler et al., 1998; Carbajal and Schaeffer, 1999; Wojciak-Stothard et al., 2001). These effects of thrombin are blocked by C3 exoenzyme. Consistent with

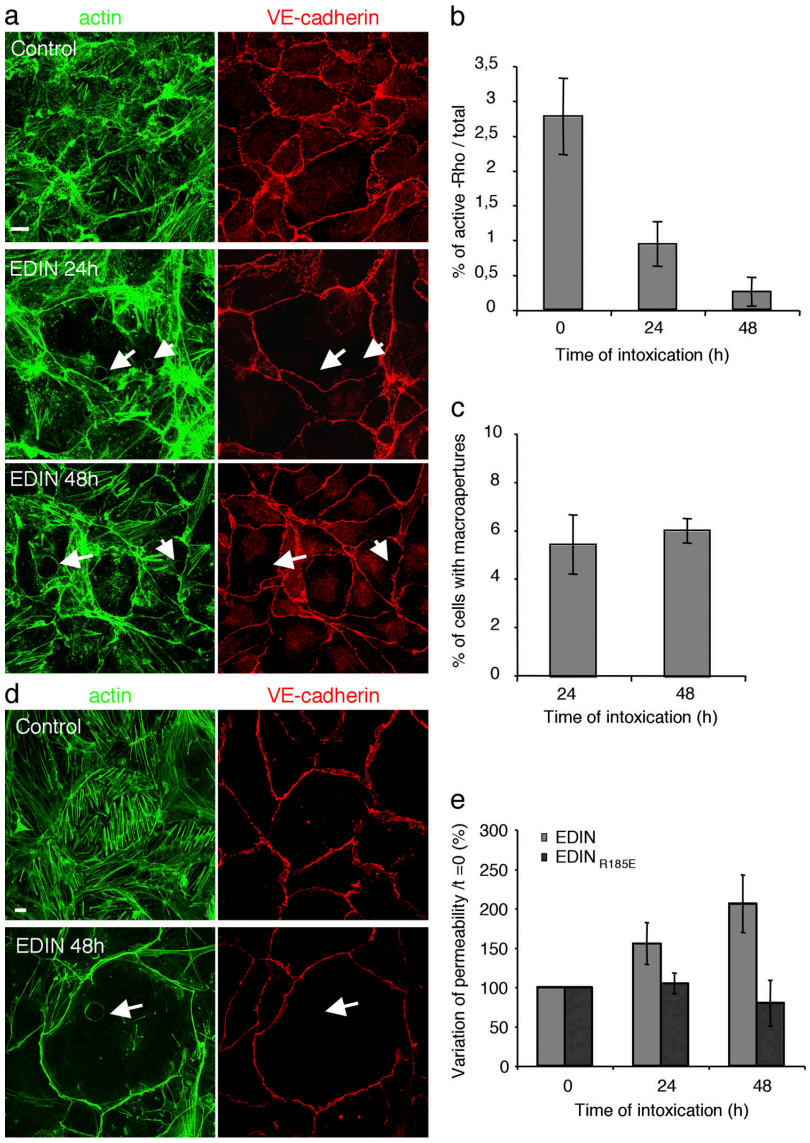

Figure 5. **Effect of EDIN on endothelial monolayers.** (a) Disruption of actin stress fibers and formation of MAs in HUVECs monolayers intoxicated with 100 μg/ml of EDIN during the indicated periods of time. Monolayers were labeled with FITC-phalloidin (actin), together with anti-cadherin5 (VE-cadherin). Arrows indicate MA location. (b) Levels of active Rho were determined by GST-rhotekin RBD pull-down assay. Values of active Rho are expressed by comparison with the signal obtained with 2% of total Rho; t = 0. Mean values ± SD. $n = 3$. (c) Percentages of HUVECs displaying at least one MA were determined on FITC-phalloidin–labeled cells in two independent experiments and expressed as mean values ± SD. (d) Effect of EDIN on HMVEC monolayers, as described in a. (e) Effects of EDIN and $EDIN_{R185E}$ on endothelial monolayer barrier function were assessed at the indicated periods of time, by determining quantities of flow through of FITC-BSA from the top to bottom chamber. Graph represents percentages of variation of permeability, as compared with t = 0 of each monolayer. Mean ± SD. $n = 4$. Bars, 10 μm.

previous findings, we measured that short periods of intoxication by EDIN or C3 exoenzyme efficiently blocked the thrombin-induced activation of RhoA, the formation of intercellular gaps and an increase of monolayer permeability, whereas it did not efficiently inhibit the level of active-Rho (Fig. S3). Longer periods of intoxication were necessary to lower the level of active Rho required to produce MAs and to compromise monolayer barrier function (Fig. 5, b and e).

Collectively, our results were indicative of a role of EDIN in producing MAs in the endothelium. We addressed this question by analyzing the effects produced by purified recombinant EDIN on the endothelium of rat arteries. The lumenal surface of arteries was analyzed by scanning electron microscopy 7 h after intoxication with either purified recombinant EDIN or with the catalytic-inactive mutant $EDIN_{R185E}$ (Fig. 6). We specifically observed MAs at the surface of the endothelium of EDIN-intoxicated arteries (Fig. 6, a and b). EDIN-intoxicated arteries had 400 ± 50 MAs/mm^2 at their surface. Consistent with our observations of endothelial cells, we observed a high heterogeneity of the size of these MAs with a mean value of 7 ± 3 μm (n = 50 MAs, at 7 h of intoxication). MAs were found to unmask the fibrous structure of the extracellular matrix visualized underneath the endothelium (Fig. 6 c). In parallel, we observed by transmission electron microscopy that EDIN disrupted the endothelial cell layer integrity (Fig. 6 d). Finally, investigating the effects of Rho ADP-ribosylating toxins on vascular permeability using a classical Evans blue dye extravasation assay in mice, we found that EDIN and C3 exoenzyme induced dye diffusion (Fig. 6 e; and Fig. S3, d and e). Collectively, our results show that Rho inactivation produces MAs in the endothelium and compromises the endothelium barrier function.

S. aureus producing EDIN get access to the endothelial basement membrane

We next addressed the question of whether the effects of EDIN might confer to *S. aureus* a physical mechanism by which the endothelium basement membrane is exposed to the bacteria. To address this question, *S. aureus* S25-*edin*$^-$ and -*edin*$^+$ strains

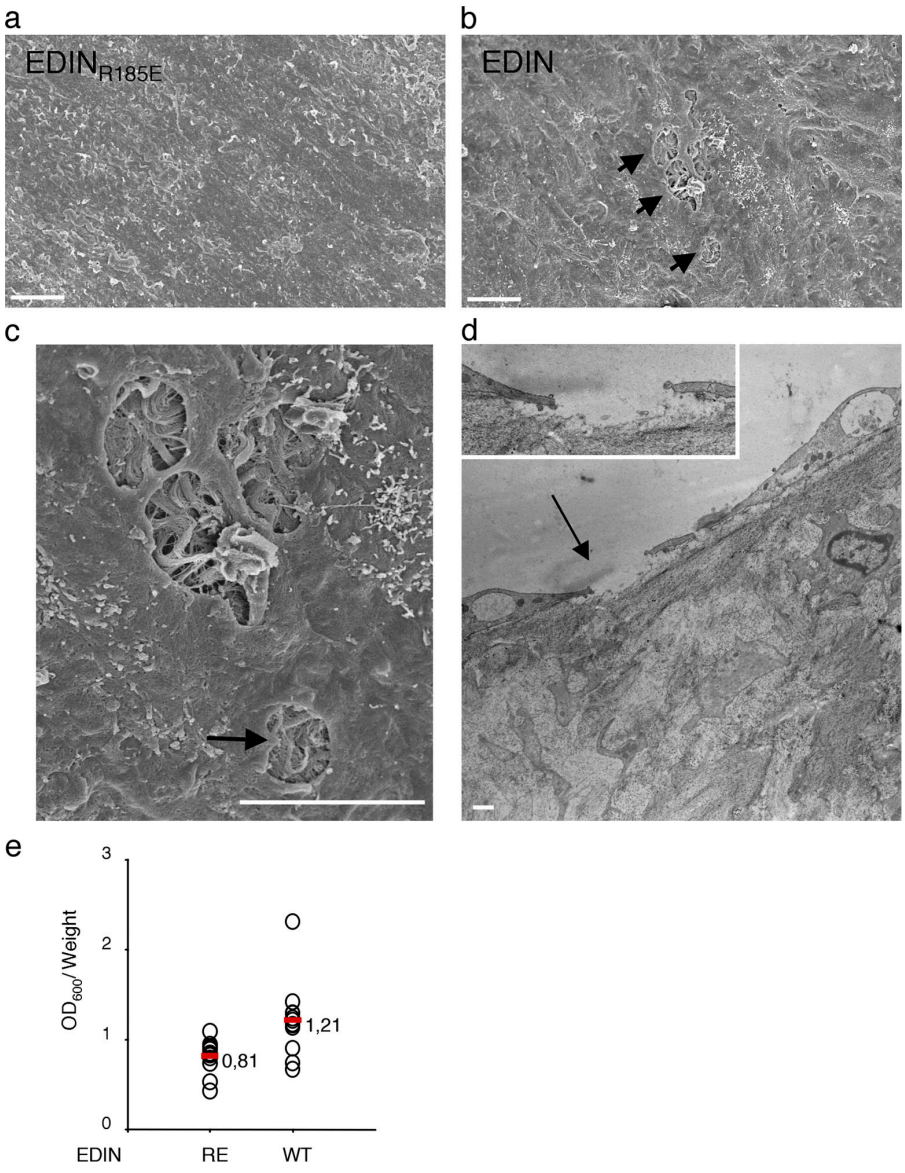

Figure 6. **MA formation on aortic endothelium induced by EDIN.** (a–d) Rat aortic arteries were intoxicated for 7 h with 200 μg/ml of either EDIN or $EDIN_{R185E}$. MAs at the surface of the endothelium were visualized by scanning electron microscopy using lower detector conditions SEI (a–c) and by transmission electron microscopy (d). (c) Formation of MAs unmasks the fibrous structure of endothelial cell adhesive matrix molecules. (d) Section of intoxicated arteries analyzed by transmission electron microscopy. (e) Quantification of the effects of C3 exoenzyme (C3) on vascular extravasation of Evans blue dye in ears (one representative experiment out of three). Groups of mice had either wild-type EDIN or mutated $EDIN_{RE}$ injected into the tail vein 36 h before Evans blue injection. Graph represents OD_{600} values of Evans blue dye extracted and normalized to tissue weight (each circle corresponds to one ear). Red lines correspond to mean values. $P < 0.006$, t test. Bars: (a–c) 10 μm; (d) 1 μm.

were engineered from the EDIN-producing human pathogenic strain S25. We verified in these strains the presence of an EDIN-encoding gene, as well as the RhoA ADP-ribosylation activity (Fig. S4, available at http://www.jcb.org/cgi/content/full/jcb.200509009/DC1). After MA formation in HUVECs that were infected by these different strains of *S. aureus*, we determined that EDIN was specifically required for actin stress fiber disruption and MA induction (Fig. 7 a). The transient formation of MAs in HUVECs infected by wild-type S25 was also verified (Video 10). We went on to determine the biological effects of EDIN on the endothelium of rat arteries infected by *S. aureus*. We observed that both wild-type S25 and S25-*edin*$^+$ strains, in contrast to S25-*edin*$^-$, produced MAs in the endothelium (Fig. 7 b). The surface of the endothelium also appeared smoother after infection by EDIN-producing *S. aureus*. Consistent with our hypothesis, EDIN-producing bacteria were observed in close proximity to the endothelium basement membrane (Fig. 7 c).

Discussion

We report that inactivation of RhoA, either by ADP-ribosylating factors or by cellular depletion, leads to the formation of large and transient transcellular tunnels within endothelial cells that we have named MAs. We show that these structures compromise the integrity of the endothelium barrier.

The observation that EDIN induces both actin cable disruption and a formation of MAs favor a scenario in which the specific inactivation of RhoA by EDIN first leads to actin cable disruption, which in turn allows formation of transcellular MAs. Consistently, we show that MAs are formed through RhoA depletion by RNAi knockdown and ROCK inhibition, as well as actin filament disassembly with cytochalasin D and latrunculin B. EDIN did not affect the levels of active Rac or Cdc42 (unpublished data). The importance of the specificity of RhoA inhibition in inducing the formation of MAs is reinforced by the observation that inhibitors that affect several Rho proteins, such as RhoGDI or *C. difficile* toxin-B, produced cell retractions instead of MAs. We have noticed that high concentrations of the ROCK inhibitory molecule Y-27632 are required to produce MAs. Thus, we cannot exclude the implication of other RhoA-regulated pathways in EDIN-induced MA formation. One likely hypothesis is that destruction of thin actin stress fibers through inactivation of the RhoA–mDIA pathway contributes to MA formation (Watanabe et al., 1999). We demonstrate that EDIN produces a specific destruction of the actin cytoskeleton network regulated by RhoA, which accounts for the formation of MAs in endothelial cells.

One question, which remains to be addressed, concerns the initial membrane events leading to the formation of MAs. One hypothesis is that MAs are initiated by ruptures of the plasma membrane. This is unlikely, considering that EDIN did not trigger Lamp1 localization at the plasma membrane like membrane wounding does (Huynh et al., 2004). Alternatively, formation of MAs could be caused by either a fusion of vesicles and/or plasma membranes or to the enlargement of a preexisting pore. In line with this last hypothesis, endothelial cells are extremely thin and

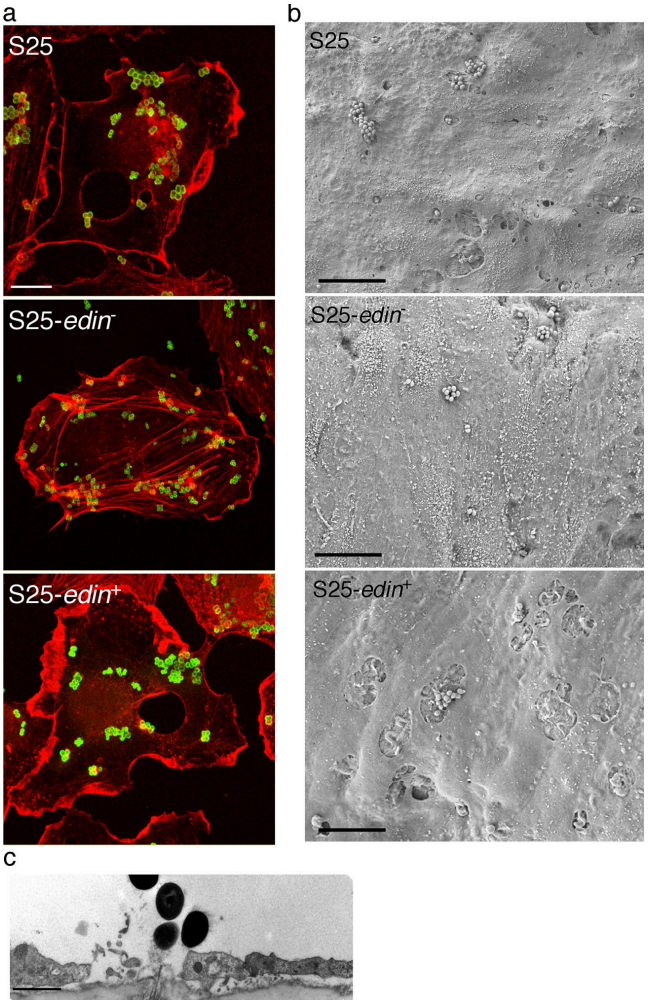

Figure 7. **EDIN-producing *S. aureus* induces MAs in endothelial cells.** (a) Visualization of the actin cytoskeleton and bacteria using TRITC-conjugated phalloidin and rabbit serum anti–*S. aureus* (green), respectively. HUVECs were infected for 1 h with S25, S25-*edin*$^+$, or -*edin*$^-$ strains of *S. aureus* at a MOI of 100. (b) Lumenal surface of infected arteries visualized by scanning electron microscopy. Rat aortic arteries were infected for 1 h with S25, S25-*edin*$^+$, or -*edin*$^-$ strains of *S. aureus* at 10^6 bacteria/ml. Scanning electron microscopy pictures were acquired using the microscope's lower detector conditions. (c) Transmission electron microscopy picture showing EDIN-producing *S. aureus* located in contact with the endothelium basement membrane. Rat aortic arteries were infected for 1 h with 10^6 wild-type S25 bacteria/ml. Bars: (a and b) 10 μm; (c) 1 μm.

are rich in interconnected vesicles referred to as vesiculo-vacuolar organelles (VVO), which provide a route of extravasation of macromolecules that is induced by the vascular permeability factor VEGF, for example (for review see Dvorak and Feng, 2001). Formation of MAs through enlargement of VVO structures seems unlikely, considering that cotreatment of EDIN-intoxicated endothelial cells with VEGF did not increase the rate of MA formation (unpublished data), and that MAs form in cell types other than endothelial cells. Finally, it is possible that MAs initiate through luminal and abluminal membrane fusion. Notably, plasma membrane fusions occur during daughter cell partitioning, which is a biological phenomenon in which the completion of cytokinesis may require the down-regulation of RhoA (Jantsch-Plunger et al., 2000). Bridging luminal and

abluminal plasma membranes might favor formation of MAs. In line with this latter hypothesis, high intravascular pressures lead to the formation of intracellular gaps in endothelial cells (Neal and Michel, 1996). Hence, it has been previously reported that RhoA ADP-ribosylation induces cell spreading, which is a phenomenon that may favor the contact between luminal and abluminal plasma membranes (Carbajal and Schaeffer, 1999). In line with this last hypothesis, we have measured that EDIN produced less MAs when endothelial cells are buried in monolayers, as compared with subconfluent cells.

Different types of structures account for endothelium permeability (for review see Michel and Curry, 1999). Majno and Palade (1961) first observed that the increase in microvascular permeability is achieved by formation of gaps between endothelial cells. Nevertheless, ultrastructural studies have shown that other types of gaps, which are referred to as openings, pass through, rather than between, endothelial cells (Feng et al., 1997; Michel and Neal, 1999). Finally, recent works suggest that endothelium permeability also results from the formation of VVO structures, in the absence of either inter- or intracellular gap formation (Dvorak and Feng, 2001). RhoA activation and the downstream contraction of the actin cytoskeleton has been recognized as a central element of intercellular gap formation in response to vasoactive mediators such as thrombin (Essler et al., 1998; Carbajal and Schaeffer, 1999; Wojciak-Stothard and Ridley, 2002). Consistent with this notion, blocking the thrombin-induced activation of RhoA using Rho ADP-ribosylating C3 exoenzyme impairs the increase of endothelial monolayer permeability (Wojciak-Stothard et al., 2001). We report that a higher threshold of inactivation of RhoA allows MA formation in endothelial cells and impacts endothelial monolayer barrier function. Collectively, these findings point to the activation or inactivation of RhoA, leading to either inter- or intracellular gap formation. The relative contribution of inter- and intracellular gaps in the regulation of the endothelium permeability is under debate (Michel and Neal, 1999). One hypothesis is that the formation of MAs represents a favorable pathway for inflammatory cell emigration from the blood stream. This idea is supported by the observations that inflammatory cells can migrate across thinner areas of endothelial cells that are distant from intercellular junctions during their extravasation from the blood stream (Feng et al., 1997; Hoshi and Ushiki, 1999). In vitro studies indicate that during their diapedesis inflammatory cells trigger the formation of membrane projections or transmigratory cups in endothelial cells (Carman and Springer, 2004; Millan and Ridley, 2005). Transmigratory cups show similarities with the MAs surrounded by membrane waves induced by EDIN. In line with possible similarities between both phenomenons, membrane projections formed during leukocyte transmigration were not blocked upon RhoA ADP-ribosylation, whereas they were blocked upon inhibition of Rho proteins by *C. difficile* toxin-B (Carman and Springer, 2004). Thus, it will be interesting to determine whether the complex crosstalk of leukocytes with endothelial cells triggers a local inhibition of RhoA for transmigratory cup formation, and whether EDIN has exploited this regulation to induce the formation of MAs.

Little is known concerning the role of EDIN with regard to human infection by *S. aureus*, except that pathogenic *S. aureus* have a higher prevalence of *edin* genes, as compared with nasal isolates (Czech et al., 2001). This Gram-positive bacterium colonizes the epithelium in 30–50% of healthy adults worldwide. Its ability to produce bacteremia on accidental or surgical wounds can lead to severe endovascular and metastatic infections (Lowy, 1998). Development of such serious infections requires numerous bacterial virulence factors, comprising microbial surface components recognizing endothelial cell–adhesive matrix molecules (Foster and Hook, 1998; Lowy, 1998). The mechanism by which luminally located *S. aureus* accesses components of the endothelial cell basement membrane remains an outstanding question. Based on our observations, it can be hypothesized that MA formation may provide EDIN-producing *S. aureus* with a specific mechanism to induce a discontinuity of the endothelium barrier.

Materials and methods

DNA constructs and bacterial genetic

The DNA encoding EDIN (NCBI M63917) was cloned using EcoRI–XhoI into pcDNA4 (Invitrogen) after PCR amplification on the E1 strain of *S. aureus* (provided by M. Sugai, Hiroshima University, Hiroshima, Japan; Inoue et al., 1991) using the following oligonucleotides: E1r, 5′-CCCGAATTCATGAAAAACAAATTACTTTTTAAAATTTTTTTG-3′ and E1f, 5′-CCCCTCGAGCTATTTTTTAAAAACAATAGCTGTTATTATG-3′. For EDIN production, the DNA was cloned using BamHI–EcoRI into pET28a after PCR amplification using oligonucleotides 5′-CCGGATCCGCTGATGTTAAAAATTTCACTGATTTAG-3′ and 5′ GGGAATTCCTATTTTTTAAAAACAATAGCTGTTATT-3′. For expression in *S. aureus*, *edin* was cloned using BamHI–PstI into pMK4-pPROT (Archambaud et al., 2005) after PCR amplification using oligonucleotides E1r, 5′-CCCGGATCCATGAAAAACAAATTACTTTTTAAAATTTTTTTG-3′ and E1f, 5′-CCCCTGCAGCTATTTTTTAAAAACAATAGCTGTTATTATG-3′. Recombinant bacterial strains were generated from an EDIN-producing human pathogenic strain of *S. aureus* (labeled S25) isolated from a 75-yr-old man with a spondylodiscitis-associated bacteremia (P. Boquet and P. Dellamonica, Hôpital ARCHET II, Nice, France). The S25-*edin*$^{+}$ strain was generated by introducing the pMK4-pPROT-*edin* into the S25-*edin*$^{-}$ strain corresponding to wild-type S25 cured of EDIN-encoding plasmid, using standard protocols. These strains were checked for the presence of an *edin*-encoding gene (using oligonucleotides E1r and E1f), as well as for ADP-ribosylation activity of RhoA (Fig. S4). The pEF-C3 was used for expression into cells of *C. botulinum* C3 exoenzyme (Hill et al., 1995). The DNAs encoding EDIN-B (NCBI AJ277173) and EDIN-C (NCBI NC_003265) were isolated after PCR amplification of pathogenic strains of *S. aureus* isolated at the Hospital of Nice (Nice, France; strains 7256 and Stal36, respectively). The DNAs of *edin*-B and -C were cloned using BamHI–EcoRI into pcDNA4 (Invitrogen) after being amplified using the following oligonucleotides: B, 5′-CCGGATCCATGGCCGAGACTAAAAATTTACAGACTTAGTT-3′ and 5′-GGGAATTCTTATTTTTTAAAAACTACAGCAGTTATAAT-3′ or C, 5′-GGGGATCCATGAAAAGAAAATTATTTTTTAAAATT-3′ and 5′-GGGAATTCTTACTTTTTGAAAACGATACCTTCGAT-3′. Mutation R185E in the conserved sequence GRPI of EDIN, and the equivalent in EDIN-B, -C, and the C3 exoenzyme were introduced by changing AGA into GAA (EDIN), AGG into GAG (EDIN-B), AGA into GAA (EDIN-C), and AAG into GAG (C3 exoenzyme) using the QuickChange site directed mutagenesis kit (Stratagene). A previously described *rhoA* RNAi sequence (5′-AAGGCAGAGAUAUGGCAAACA-3′) or a corresponding *rhoA* RNAi scrambled sequence (control RNAi; 5′-GAAGTGACGACAGGACAAATA-3′) were cloned in the pSIRNA vector (Invivogen) according to the manufacturer's instructions. Human β-actin cDNA was cloned using XhoI–ApaI in pEGFP-C1 (CLONTECH Laboratories, Inc.). pCMV-RFP-actin was provided by E. Fuchs (The Rockefeller University, New York, NY). Other DNA constructs used were pDsRed2-Nuc (CLONTECH Laboratories, Inc.), canis Caveolin1 cloned using XhoI–BamHI in pEGFP-C1, rattus Lamp1 cloned using XhoI–BamHI into pEGFP-N2, human RhoGDI-α 6His-tagged cloned using BglII–PstI in pCMV (pRhoGDI), and VE-cadherin cloned using EcoRI–BamHI in pEGFP-N3 (provided by D. Gulino, Institut de Biologie Structurale Jean-Pierre Ebel, Grenoble, France).

Cell culture and biochemical products

HUVECs (PromoCell) were grown in serum-free medium (SFM) supplemented with 20% FBS, 20 ng/ml basic FGF, 10 ng/ml EGF (Invitrogen), and 1 μg/ml heparin (Sigma-Aldrich). HUVECs were electroporated as previously described (Doye et al., 2006), using 5 μg pDsRed2-Nuc together with 10 μg of pEDIN for toxin expression. For subconfluent HUVEC experiments, cells were plated at 15,000 HUVECs per well in 12-well plates. Human primary keratinocytes and fibroblasts were provided by L. Turchi (Faculté de Médecine, Nice, France). HMVECs (provided by A. Orecchia and G. Zambruno, Instituto Dermopatico dell'Immacolata–Instituto di Ricovero e Cura a Carattere Scientifico, Rome, Italy) were isolated and grown as previously described (Jackson et al., 1990). Other cells used were Saos-2 epithelial cells derived from osteosarcoma (HTB-85), L6 myoblast cells (CRL-1458), and VERO epithelial cells derived from kidney (CCL-81; all from American Type Culture Collection). C3 exoenzyme and EDIN were purified by His-tag affinity chromatography. EDIN was further dialyzed against 25 mM Tris and 50 mM NaCl, and then purified on a CM–Sepharose fast flow (GE Healthcare). The antibodies used were monoclonal anti-RhoA, anti-Cdc42, and anti-Rac1 (BD Biosciences), anti-GFP (clones 7.1 and 13.1; Roche), anti–β-actin (clone AC-74; Sigma-Aldrich), anti-cortactin (clone 4F11; Upstate Biotechnology), polyclonal anti-cadherin5 (Bender MedSystems), and allophycocyanin-conjugated anti-Lgp120/Lamp1 (clone H4A3; Abcam). Arp3 polyclonal antibodies were provided by P. Cossart (Institut Pasteur, Paris, France). Anti–*S. aureus* serum was raised against the E-1 strain (Sugai et al., 1990) using standard rabbit immunization protocols (Eurogentec). For immunofluorescence analysis, primary antibodies were visualized using Texas red–conjugated anti–mouse antibodies (Vector Laboratories), Texas red–conjugated anti–rabbit antibodies (Jackson ImmunoResearch Laboratories), or FITC-conjugated anti–rabbit antibodies (Biosys). For immunoblotting, primary antibodies were visualized using goat anti–mouse or anti–rabbit horseradish peroxidase–conjugated secondary antibodies (DakoCytomation), followed by chemiluminescence detection ECL (GE Healthcare). Biochemical products were purchased from Sigma-Aldrich, with the exception of latrunculin B and cytochalasin D (Calbiochem). The toxin-B of *C. difficile* was provided by I. Just (Hannover Medical School, Hannover, Germany).

Transendothelial and in vivo permeability assays

For permeability assays, HUVECs were grown on gelatin-coated polyester filters (3-μm pore size; 12-mm diam; Greiner Bio-One). Cells were plated at 2×10^5 cells/well and grown for 4 d in supplemented SFM. For intoxication, HUVEC monolayers were treated with 100 μg/ml of EDIN or $EDIN_{R185E}$ in supplemented SFM. For thrombin treatment, monolayers were incubated 1 h with thrombin 1 U/ml in SFM. Variations of permeability of each monolayer were followed at different periods of time (0, 24, and 48 h). In brief, at each time point the medium in the top chamber was replaced by supplemented SFM containing 0.5 mg/ml FITC-BSA (Invitrogen). Samples were collected after 10 min in the bottom compartments. Monolayers were washed once and incubated again in supplemented SFM containing toxin up to the next measurements. Levels of FITC-BSA in the bottom chamber were determined with a fluoroscan Ascent (Thermolab System), using an excitation wavelength of 485 nm, and detecting emission at 538 nm. Animal vascular permeability was assessed using a classical Evans blue dye extravasation assay. Groups of 6-wk-old BALB/c mice were injected into the tail vein three times at 12 h intervals, with 5 or 10 mg of toxins/Kg (for C3 or EDIN). Evans blue dye (30 mg/Kg in 100 μl PBS; Sigma-Aldrich) was injected into the tail vein 36 h after the first injection, and the Evans blue dye was extracted 1 h later from ears and quantified, as previously described (Han et al., 2002). Animals used during this study were maintained and handled according to the regulations of the European Union and the French Department of Health and Agriculture.

Microscopy techniques and video imaging

Immunofluorescence studies were performed on cells fixed in 4% paraformaldehyde (Sigma-Aldrich). The actin cytoskeleton was labeled using 1 μg/ml FITC- or TRITC-conjugated phalloidin (Sigma-Aldrich). For plasma membrane labeling, intact cells were incubated with 20 μg/ml FITC-conjugated WGA (Sigma-Aldrich) at 4°C before fixation. Immunosignals were analyzed with a confocal microscope (TCS-SP; Leica) with a 63× magnification lens. Each picture represents the projection of four serial confocal sections. Cells were analyzed by video microscopy on an Axiovert 200 microscope equipped with shutter-controlled illumination (Carl Zeiss MicroImaging, Inc.) and a cooled digital charge-coupled device camera (Roper Scientific). Images were processed using MetaMorph 2.0 image analysis software (Invitrogen) and QuickTime pro 7 software (Apple).

For electron microscopy, 6–8 wk old male Wistar rats (150–200 g; Janvier Laboratories) were anesthetized with pentobarbital (30 mg/kg i.p.) and ketamine (100 mg/kg i.p.) before i.v. injection of 10 mg/kg heparin (Sigma-Aldrich). 5-mm-long aortic arches were excised and rinsed in Celsior medium (Imtix-Sangstat) supplemented with 0.1% wt/vol heparin. Arteries were incubated for 7 h at 37°C in Celsior supplemented with 0.2 μg/ml of purified recombinant EDIN or $EDIN_{R185E}$ or for 1 h with *S. aureus* strains. Samples were removed and immersed in 1.5% glutaraldehyde in 100 mM phosphate buffer, pH 7.4, for at least 18 h at 4°C, and then processed in parallel for transmission electron microscopy (CM12; Philips) and scanning electron microscopy (6340F; Jeol), using standard techniques (Arnold and Boor, 1986). Animals used during this study were maintained and handled according to the regulations of the European Union and the French Department of Health and Agriculture.

Biochemical assays

For ADP-ribosylation assays, control or intoxicated HUVECs (10^7 cells/time point) were homogenized in 0.25 ml cold BSI buffer (3 mM imidazole, pH 7.4, and 250 mM sucrose) supplemented extemporaneously with 1 mM phenylmethylsulfonyl fluoride. Cells were lysed by passing 40 times through a 1-ml syringe equipped with a 25G × 5/8″ needle (U-100 Insulin; Terumo Medical Corporation). Nuclei were removed by centrifugation for 10 min at 10,000 *g* at 4°C. Protein concentrations of the postnuclear supernatants were determined using DC protein assay (Bio-Rad Laboratories). ADP-ribosylations were performed for 30 min at 37°C on 10 μg of intoxicated cell lysates supplemented with 0.5 μCi [^{32}P]NAD (800 Ci/mmol) and 1 μg of EDIN. Levels of active Rho were determined by GST-rhotekin RBD pull-down that was modified as described previously (Doye et al., 2002).

Online supplemental material

Fig. S1 shows actin cytoskeleton disruption and MA formation by EDIN-isoforms. Fig. S2 shows the effect of EDIN on HUVECs expressing GFP-actin. Fig. S3 shows the interference of EDIN on thrombin-induced increase of monolayer permeability. Fig. S4 is a characterization of S25-derived *S. aureus* strains. Video 1 shows endothelial cell intoxication by EDIN. Video 2 shows EDIN intoxication of HUVECs expressing GFP-caveolin1. Video 3 shows VERO cell intoxication by EDIN. Video 4 shows endothelial cell intoxication by C3-exoenzyme of *C. botulinum*. Video 5 shows actin dynamics in *rhoA* RNAi transfected HUVECs. Video 6 shows actin dynamics in EDIN-intoxicated endothelial cells. Video 7 shows HUVEC intoxication by toxin-B of *C. difficile*. Video 8 shows the effect of EDIN on endothelial cells expressing VE-cadherin–GFP and RFP-actin in the monolayer. Video 9 shows the effect of EDIN on the endothelial cell monolayer. Video 10 shows HUVEC infection by *S. aureus*. Online supplemental material is available at http://www.jcb.org/cgi/content/full/jcb.200509009/DC1.

We wish to thank Y. Le Marchand-Brustel for sharing the video microscopy facility (a donation of the Bettencourt-Schueller's Foundation to Institut National de la Santé et de la Recherche Médicale [INSERM] U568), P. Boquet and P. Dellamonica for help in screening pathogenic strains of *S. aureus*, and E. Van Obberghen (INSERM U145) for animal facilities. We thank A. Cheung, B. Faivre, N. Gautier, C. Hinault, T. Juhel, J.P. Laugier, C. Neveu, S. Pagnotta, and T. Yandza for technical assistance. We thank P. Hare and M. Mhlanga for comments on the manuscript. We thank A. Grima for infography assistance.

Our laboratory is supported by institutional funding from INSERM, a grant (ANR A05135AS) from the Agence Nationale de la Recherche, a grant from the Association pour la Recherche sur le Cancer (ARC 3337), and a fellowship to L. Boyer from the Ligue Nationale Contre le Cancer.

Submitted: 2 September 2005
Accepted: 5 May 2006

References

Aktories, K., C. Wilde, and M. Vogelsgesang. 2004. Rho-modifying C3-like ADP-ribosyltransferases. *Rev. Physiol. Biochem. Pharmacol.* 152:1–22.

Archambaud, C., E. Gouin, J. Pizarro-Cerda, P. Cossart, and O. Dussurget. 2005. Translation elongation factor EF-Tu is a target for Stp, a serine-threonine phosphatase involved in virulence of *Listeria monocytogenes*. *Mol. Microbiol.* 56:383–396.

Arnold, J.R., and P.J. Boor. 1986. Improved transmission electron microscopy (TEM) of cultured cells through a "floating sheet" method. *J. Ultrastruct. Mol. Struct. Res.* 94:30–36.

Bazzoni, G., and E. Dejana. 2004. Endothelial cell-to-cell junctions: molecular organization and role in vascular homeostasis. *Physiol. Rev.* 84:869–901.

Boquet, P., and E. Lemichez. 2003. Bacterial virulence factors targeting Rho GTPases: parasitism or symbiosis? *Trends Cell Biol.* 13:238–246.

Burridge, K., and K. Wennerberg. 2004. Rho and Rac take center stage. *Cell*. 116:167–179.

Carbajal, J.M., and R.C. Schaeffer Jr. 1999. RhoA inactivation enhances endothelial barrier function. *Am. J. Physiol.* 277:C955–C964.

Carman, C.V., and T.A. Springer. 2004. A transmigratory cup in leukocyte diapedesis both through individual vascular endothelial cells and between them. *J. Cell Biol.* 167:377–388.

Caron, E., and A. Hall. 1998. Identification of two distinct mechanisms of phagocytosis controlled by different Rho GTPases. *Science*. 282:1717–1721.

Chardin, P., P. Boquet, P. Madaule, M.R. Popoff, E.J. Rubin, and D.M. Gill. 1989. The mammalian G protein rhoC is ADP-ribosylated by *Clostridium botulinum* exoenzyme C3 and affects actin microfilaments in Vero cells. *EMBO J.* 8:1087–1092.

Czech, A., T. Yamaguchi, L. Bader, S. Linder, K. Kaminski, M. Sugai, and M. Aepfelbacher. 2001. Prevalence of Rho-inactivating epidermal cell differentiation inhibitor toxins in clinical *Staphylococcus aureus* isolates. *J. Infect. Dis.* 184:785–788.

DerMardirossian, C., and G.M. Bokoch. 2005. GDIs: central regulatory molecules in Rho GTPase activation. *Trends Cell Biol.* 15:356–363.

Doye, A., A. Mettouchi, G. Bossis, R. Clement, C. Buisson-Touati, G. Flatau, L. Gagnoux, M. Piechaczyk, P. Boquet, and E. Lemichez. 2002. CNF1 exploits the ubiquitin-proteasome machinery to restrict Rho GTPase activation for bacterial host cell invasion. *Cell*. 111:553–564.

Doye, A., L. Boyer, A. Mettouchi, and E. Lemichez. 2006. Ubiquitin-mediated proteasomal degradation of Rho Proteins by the CNF1 Toxin. *Methods Enzymol.* 406:447–456.

Dvorak, A.M., and D. Feng. 2001. The vesiculo-vacuolar organelle (VVO). A new endothelial cell permeability organelle. *J. Histochem. Cytochem.* 49:419–432.

Essler, M., M. Amano, H.J. Kruse, K. Kaibuchi, P.C. Weber, and M. Aepfelbacher. 1998. Thrombin inactivates myosin light chain phosphatase via Rho and its target Rho kinase in human endothelial cells. *J. Biol. Chem.* 273:21867–21874.

Feng, D., J.A. Nagy, J. Hipp, K. Pyne, H.F. Dvorak, and A.M. Dvorak. 1997. Reinterpretation of endothelial cell gaps induced by vasoactive mediators in guinea-pig, mouse and rat: many are transcellular pores. *J. Physiol.* 504:747–761.

Foster, T.J., and M. Hook. 1998. Surface protein adhesins of *Staphylococcus aureus. Trends Microbiol.* 6:484–488.

Fujihara, H., L.A. Walker, M.C. Gong, E. Lemichez, P. Boquet, A.V. Somlyo, and A.P. Somlyo. 1997. Inhibition of RhoA translocation and calcium sensitization by in vivo ADP-ribosylation with the chimeric toxin DC3B. *Mol. Biol. Cell*. 8:2437–2447.

Genth, H., R. Gerhard, A. Maeda, M. Amano, K. Kaibuchi, K. Aktories, and I. Just. 2003. Entrapment of Rho ADP-ribosylated by *Clostridium botulinum* C3 exoenzyme in the Rho-guanine nucleotide dissociation inhibitor-1 complex. *J. Biol. Chem.* 278:28523–28527.

Han, E.D., R.C. MacFarlane, A.N. Mulligan, J. Scafidi, and A.E. Davis III. 2002. Increased vascular permeability in C1 inhibitor-deficient mice mediated by the bradykinin type 2 receptor. *J. Clin. Invest.* 109:1057–1063.

Hill, C.S., J. Wynne, and R. Treisman. 1995. The Rho family GTPases RhoA, Rac1, and CDC42Hs regulate transcriptional activation by SRF. *Cell*. 81:1159–1170.

Hoshi, O., and T. Ushiki. 1999. Scanning electron microscopic studies on the route of neutrophil extravasation in the mouse after exposure to the chemotactic peptide N-formyl-methionyl-leucyl-phenylalanine (fMLP). *Arch. Histol. Cytol.* 62:253–260.

Huynh, C., D. Roth, D.M. Ward, J. Kaplan, and N.W. Andrews. 2004. Defective lysosomal exocytosis and plasma membrane repair in Chediak-Higashi/beige cells. *Proc. Natl. Acad. Sci. USA*. 101:16795–16800.

Inoue, S., M. Sugai, Y. Murooka, S.Y. Paik, Y.M. Hong, H. Ohgai, and H. Suginaka. 1991. Molecular cloning and sequencing of the epidermal cell differentiation inhibitor gene from *Staphylococcus aureus. Biochem. Biophys. Res. Commun.* 174:459–464.

Jackson, C.J., P.K. Garbett, B. Nissen, and L. Schrieber. 1990. Binding of human endothelium to Ulex europaeus I-coated Dynabeads: application to the isolation of microvascular endothelium. *J. Cell Sci.* 96:257–262.

Jaffe, A.B., and A. Hall. 2005. RHO GTPases: Biochemistry and Biology. *Annu. Rev. Cell Dev. Biol.* 21:247–269.

Jantsch-Plunger, V., P. Gonczy, A. Romano, H. Schnabel, D. Hamill, R. Schnabel, A.A. Hyman, and M. Glotzer. 2000. CYK-4: A Rho family gtpase activating protein (GAP) required for central spindle formation and cytokinesis. *J. Cell Biol.* 149:1391–1404.

Just, I., J. Selzer, M. Wilm, C. von Eichel-Streiber, M. Mann, and K. Aktories. 1995. Glucosylation of Rho proteins by *Clostridium difficile* toxin B. *Nature*. 375:500–503.

Katoh, K., Y. Kano, M. Amano, K. Kaibuchi, and K. Fujiwara. 2001. Stress fiber organization regulated by MLCK and Rho-kinase in cultured human fibroblasts. *Am. J. Physiol. Cell Physiol.* 280:C1669–C1679.

Kimura, K., M. Ito, M. Amano, K. Chihara, Y. Fukata, M. Nakafuku, B. Yamamori, J. Feng, T. Nakano, K. Okawa, et al. 1996. Regulation of myosin phosphatase by Rho and Rho-associated kinase (Rho-kinase). *Science*. 273:245–248.

Lowy, F.D. 1998. *Staphylococcus aureus* infections. *N. Engl. J. Med.* 339:520–532.

Majno, G., and G.E. Palade. 1961. Studies on inflammation. 1. The effect of histamine and serotonin on vascular permeability: an electron microscopic study. *J. Biophys. Biochem. Cytol.* 11:571–605.

Menetrey, J., G. Flatau, E.A. Stura, J.B. Charbonnier, F. Gas, J.M. Teulon, M.H. Le Du, P. Boquet, and A. Menez. 2002. NAD binding induces conformational changes in Rho ADP-ribosylating *Clostridium botulinum* C3 exoenzyme. *J. Biol. Chem.* 277:30950–30957.

Michel, C.C., and F.E. Curry. 1999. Microvascular permeability. *Physiol. Rev.* 79:703–761.

Michel, C.C., and C.R. Neal. 1999. Openings through endothelial cells associated with increased microvascular permeability. *Microcirculation*. 6:45–54.

Millan, J., and A.J. Ridley. 2005. Rho GTPases and leucocyte-induced endothelial remodelling. *Biochem. J.* 385:329–337.

Neal, C.R., and C.C. Michel. 1996. Openings in frog microvascular endothelium induced by high intravascular pressures. *J. Physiol.* 492:39–52.

Nusrat, A., M. Giry, J.R. Turner, S.P. Colgan, C.A. Parkos, D. Carnes, E. Lemichez, P. Boquet, and J.L. Madara. 1995. Rho protein regulates tight junctions and perijunctional actin organization in polarized epithelia. *Proc. Natl. Acad. Sci. USA*. 92:10629–10633.

Paterson, H.F., A.J. Self, M.D. Garrett, I. Just, K. Aktories, and A. Hall. 1990. Microinjection of recombinant p21rho induces rapid changes in cell morphology. *J. Cell Biol.* 111:1001–1007.

Roy, D., D.R. Liston, V.J. Idone, A. Di, D.J. Nelson, C. Pujol, J.B. Bliska, S. Chakrabarti, and N.W. Andrews. 2004. A process for controlling intracellular bacterial infections induced by membrane injury. *Science*. 304:1515–1518.

Sugai, M., T. Enomoto, K. Hashimoto, K. Matsumoto, Y. Matsuo, H. Ohgai, Y.M. Hong, S. Inoue, K. Yoshikawa, and H. Suginaka. 1990. A novel epidermal cell differentiation inhibitor (EDIN): purification and characterization from *Staphylococcus aureus. Biochem. Biophys. Res. Commun.* 173:92–98.

Watanabe, N., T. Kato, A. Fujita, T. Ishizaki, and S. Narumiya. 1999. Cooperation between mDia1 and ROCK in Rho-induced actin reorganization. *Nat. Cell Biol.* 1:136–143.

Weed, S.A., Y. Du, and J.T. Parsons. 1998. Translocation of cortactin to the cell periphery is mediated by the small GTPase Rac1. *J. Cell Sci.* 111:2433–2443.

Wilde, C., M. Vogelsgesang, and K. Aktories. 2003. Rho-specific *Bacillus cereus* ADP-ribosyltransferase C3cer cloning and characterization. *Biochemistry*. 42:9694–9702.

Wojciak-Stothard, B., and A.J. Ridley. 2002. Rho GTPases and the regulation of endothelial permeability. *Vascul. Pharmacol.* 39:187–199.

Wojciak-Stothard, B., S. Potempa, T. Eichholtz, and A.J. Ridley. 2001. Rho and Rac but not Cdc42 regulate endothelial cell permeability. *J. Cell Sci.* 114:1343–1355.